Predictive Tool To Aid Design and Operations of Pressurized Fixed Bed Coal Gasifiers

Esmail R. Monazam

Department of Mechanical and Aerospace Engineering, West Virginia University, Morgantown, West Virginia 26505

Lawrence J. Shadle*

U.S. Department of Energy, Federal Energy Technology Center, P.O. Box 880, Morgantown, West Virginia 26507-0880

A mathematical model is presented to study the combustion and gasification of char with air and steam under pressure. A series of curves was obtained from the solutions of energy and mass balances for the probable range of operation in the gasification of char. Certain theoretical conclusions are drawn with respect to gasification of char in a fixed bed and found to be in accord with the results of the literature. A mathematical correlation is presented for conveniently calculating the product gas composition, the burning rate, the combustion zone thickness, the solids' maximum temperature, and the outlet gas temperature. This correlation is of general applicability, covers a wide range of operating conditions through use of multiple variance analysis, and may be used for pressures as high as 4200 kPa. Examples are given to illustrate the use and versatility of the correlation.

Introduction

Interest in research and development of coal gasification has increased due to the potential enhancement of a utility's power production efficiency using advanced power systems such as integrated gasification combined cycles. In particular, these cycles incorporate pressurized coal gasification processes. Experimental studies at the Bureau of Mines in Pittsburgh have shown that in Lurgi type pressurized gasifiers, the throughput is increased several times by gasification under pressure (Cooperman et al., 1951). In addition, Hubmann (1954) displayed that operational problems associated with coal swelling and complete agglomeration of the charge are also reduced when gasification is conducted at elevated pressures.

A gasifier model was required to evaluate the potential of a new hybrid gasifier, such as PyGas (Brown and Sadowski, 1991). PyGas is a novel air-blown pressurized gasifier (up to 4200 kPa) which integrates three reactor systems: the coal is fed into a spouting fluidized bed pyrolyzer, the char and pyrolysis products overflow onto the top of a cocurrent flow gasification and oxidation section, and then the hot char passes to a fixed bed gasification section (Figure 1). To simplify the simulation, the approach taken was to model the various stages, in detail, separately. This paper focuses on modeling the fixed bed sections of this gasifier. Since the relative velocity of the gases is much greater than that of the solids in all fixed bed systems, the model described below can accurately simulate both countercurrent and cocurrent flow systems. Because the PyGas fixed bed stages will operate using char fines introduced at elevated temperatures (rather than coal), its performance, the influence of design variables and processing conditions, was expected to vary from those of existing fixed bed gasifiers.

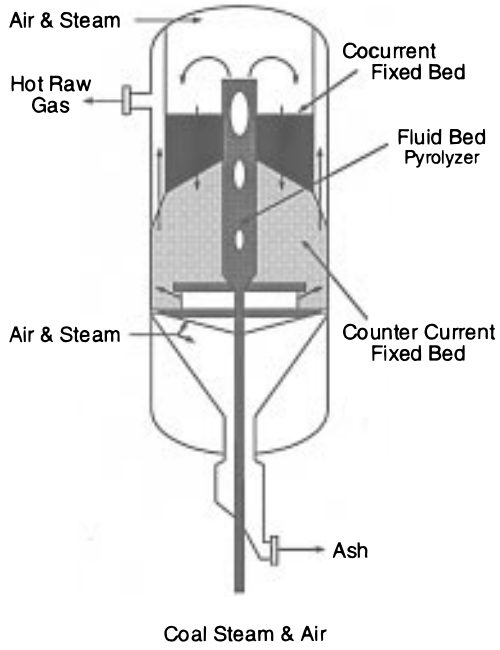

Figure 1. Schematic of proposed advanced PyGas gasifier.

Fixed bed gasification processes utilize either cocurrent, countercurrent, or cross-flow reactor configurations. In cocurrent gasifiers the fuel is fed onto the top of the fixed bed and gases flow cocurrently downward with the solids (Figure 2A). Cocurrent gasifiers are used for biomass conversion (Reed and Markson, 1983) due to the highly reactive nature of these feeds. In countercurrent gasification, more common to coal gasifiers (Cooperman et al., 1951; Hobbs et al., 1993; Wen, 1972), product gases exit from the top of the reactor where the coal is fed to dry and exchange heat with

* Author to whom correspondence should be addressed. E-mail: Lawrence.Shadle@FETC.DOE.GOV. Fax: (304)-285-4403.

S0888-5885(97)00229-7 CCC: $15.00
Published on Web 01/05/1998

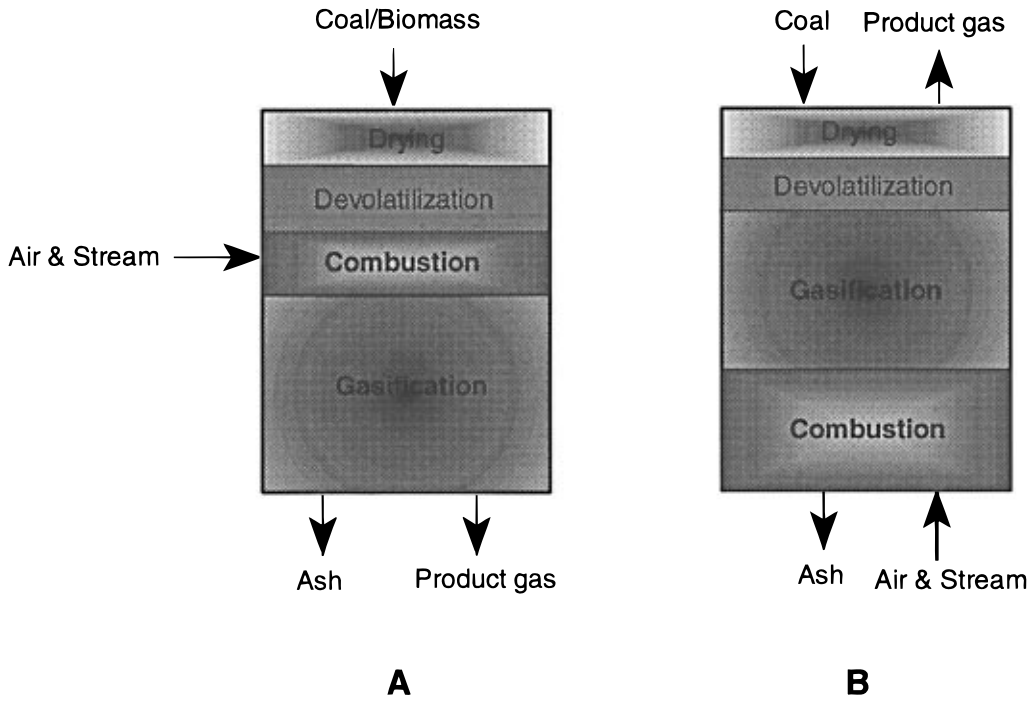

Figure 2. Simplified schematics for cocurrent (A) and countercurrent (B) fixed bed gasification processes.

these less reactive feedstocks (Figure 2B). Air and steam are fed from the bottom under a rotating grate through which residual ash and clinkers are discharged.

The first fixed bed gasification model was developed by Yoon (1978). Hobbs et al. (1993) present a comprehensive review of more recent models of fixed bed gasification. The approach adopted here was essentially based on that of Monazam et al. (1992) for a cross-current gasifier. The kinetics were the same as those presented by Wen and Chaung (1979). Past modeling efforts did not consider some peculiar aspects of the PyGas concept and thus provided no means of readily estimating performance at conditions other than those explicitly reported. Brown and Sadowski (1993) modeled the entire integrated PyGas system but in so doing sacrificed detail in the fixed bed model by assuming instantaneous and complete combustion prior to using various gasification kinetic relationships. None of these models simulated or verified the effect of elevated pressure on gasification, a key parameter in advanced power systems.

Gasification Reactions

Thermodynamic analysis of gasification systems can provide considerable insight into process feasibility. The reactions which take place in the gasifier are considered in the literature to be more or less firmly established. The fuel gases resulting from the different gasifier systems have the same essential constituents but in so widely different proportions that they vary greatly in the range and the manner of their applications. They usually embody the following combustible and noncombustible constituents in different proportions. Combustible gases include carbon monoxide (CO), hydrogen (H_2), and methane (CH_4). Noncombustible gases include carbon dioxide (CO_2), nitrogen (N_2), and water (H_2O). The combustible gases contribute to the heating value of the gas mixture, while the noncombustible gases act as diluents. The reactions that occur in a gasification reactor can be one, or any combination, of the following:

$$C + \frac{1}{\phi}O_2 \rightarrow 2\left(1 - \frac{1}{\phi}\right)CO + \left(\frac{2}{\phi} - 1\right)CO_2 \quad (1)$$

$$C + H_2O \rightarrow CO + H_2 \quad (2)$$

$$C + CO_2 \rightarrow 2CO \quad (3)$$

$$C + 2H_2 \rightarrow CH_4 \quad (4)$$

$$CO + H_2O \rightarrow CO_2 + H_2 \quad (5)$$

The oxidation of carbon (reaction 1) is highly exothermic and provides heat for the endothermic reactions (2 and 3). Reaction 1 is also extremely rapid and proceeds to completion with respect to oxygen disappearance. Reactions 2 and 3 are slow and thermodynamically favored at temperatures above 750 °C. Reaction 2 is generally considered to be slower than reaction 3 at equal concentrations of H_2O and CO_2 (Wen, 1972). The methanation of char (reaction 4) is exothermic and slow but thermodynamically favored at elevated pressure and low fuel bed temperature (<600 °C). The water−gas shift (reaction 5) is mildly exothermic with CO_2 and H_2 formation favorable below 750 °C. The water−gas shift reaction is catalyzed by a coal or char surface such that it is rapid at temperatures above 600 °C (Wen, 1972).

Model Description

For design purposes, it is necessary for the model to predict the burning rate of char and the composition

and flow of gases produced from the gasifier for a range of feed materials. Gas compositions depend on the temperature and pressure of operation, the composition of the blast (air and steam), and the contacting pattern of the blast and fuel. The approach was essentially based on that of Monazam et al. (1992). The model was a one-dimensional, adiabatic, fixed bed gasifier. The bed was considered to be a continuous solid phase of a porous nature such that gas containing air and steam can flow through it. The *y*-direction was taken as the direction of air and steam (or gas) flow, vertically upward, contacting the solid char in the bed.

The simulation was initiated by introducing the air−steam blast to the top of a preheated char bed. The initial char temperature was considered the same as those for PyGas (about 700 °C). The air and steam passed through an ash layer and burned the char particles underneath, producing hot products of combustion. The gases traveled down through the bed and gasified the char. The char particles reacted with carbon dioxide and steam to form carbon monoxide and hydrogen. These gasification reactions are extremely endothermic (except the methanation reaction).

The exchange of energy between the gas and solid phases, through conduction, convection, and radiation, was represented by a gas−solid heat transfer coefficient. The gas−solid heat transfer coefficient was assumed to be proportional to the nonreactive heat transfer coefficient taken from Gupta and Thodos (1963). This coefficient was then modified for reactive species on the basis of the physical properties of the product gases (Cho, 1980; Monazam, 1986). This approach provides a calculated heat transfer coefficient for reactive systems about 50 times less than that of the nonreactive heat transfer coefficient and is in agreement with reported values (Von Fredersdorff and Elliott, 1963).

The ash layer was assumed to remain intact on the particles. Hence, the shrinking unreacted-core model was assumed for all the heterogenous reactions (Wen, 1968) with the following expression for the rate of reaction:

$$\dot{R}''_i = \frac{(P_j - P^*_j)}{\frac{1}{K_g} + \frac{1}{K_{ash}}\left(\frac{1}{\xi} - 1\right) + \frac{1}{K_s \xi^2}} \tag{6}$$

The char−oxygen combustion reaction was modeled after that of Field et al. (1967), and the CO/CO_2 ratio was taken from Wen and Dutta (1979) and Arthur (1951). The char−carbon dioxide, char−steam, and char−hydrogen gasifications were modeled after that of Wen and Chaung (1979) using their values for the surface reaction rate constant, K_s, and the gas−solid diffusion rate constant, K_g.

The ash diffusion rate, K_{ash}, for each reaction was estimated by the correlation suggested by Wen (1972):

$$K_{ash} = K_g \epsilon_a^{2.5} \tag{7}$$

The water−gas shift reaction was assumed fast enough to be considered in equilibrium. Detailed discussion of gasification thermodynamics and kinetics is given elsewhere (Monazam et al., 1992).

On the basis of the above assumptions, the mass balances in a differential element of the reactor height, d*y*, are given by the following equations:

$$\frac{d\dot{m}''_{O_2}}{dy} = -\frac{a}{\epsilon}\frac{\tilde{M}_{O_2}}{\tilde{M}_C}\frac{1}{\Phi}\dot{R}''_1 \tag{8}$$

$$\frac{d\dot{m}''_{H_2O}}{dy} = -\frac{a}{\epsilon}\frac{\tilde{M}_{H_2O}}{\tilde{M}_C}\dot{R}''_2 \tag{9}$$

$$\frac{d\dot{m}''_{CO_2}}{dy} = \frac{a}{\epsilon}\frac{\tilde{M}_{CO_2}}{\tilde{M}_C}\left(\left(\frac{2}{\Phi} - 1\right)\dot{R}''_1 - \dot{R}''_3\right) \tag{10}$$

$$\frac{d\dot{m}''_{CO}}{dy} = \frac{a}{\epsilon}\frac{\tilde{M}_{CO}}{\tilde{M}_C}\left(\left(2 - \frac{2}{\Phi}\right)\dot{R}''_1 + \dot{R}''_2 + 2\dot{R}''_3\right) \tag{11}$$

$$\frac{d\dot{m}''_{H_2}}{dy} = \frac{a}{\epsilon}\frac{\tilde{M}_{H_2}}{\tilde{M}_C}(\dot{R}''_2 - 2\dot{R}''_4) \tag{12}$$

$$\frac{d\dot{m}''_{CH_4}}{dy} = \frac{a}{\epsilon}\frac{\tilde{M}_{CH_4}}{\tilde{M}_C}\dot{R}''_4 \tag{13}$$

$$\frac{d\xi}{dt} = -\frac{a}{3(1-\epsilon)\rho_s \xi^2}\sum_{i=1}^{4}\dot{R}''_i \tag{14}$$

Since different temperatures were used for the solid and gas, a heat balance for each phase was performed. The water−gas shift equilibrium was imposed after calculating each incremental layer, d*y*. These are the corresponding difference equations for gases

$$\sum_{j=1}^{N}\frac{\dot{m}''_{g,j}C_{pg,j}}{\tilde{M}_j}\frac{dT_g}{dy} = \frac{a}{\epsilon}\left(h(T_s - T_g) + \frac{1}{\tilde{M}_C}\sum_{i=1}^{4}\dot{R}''_i\sum_{j=1}^{N}(\hat{H}_j(T_s) - \hat{H}_j(T_g))(b_{ij} - a_{ij})\right) \tag{15}$$

and solids

$$\rho_s C_{ps}\frac{dT_s}{dt} = -\frac{a}{(1-\epsilon)}\left(h(T_s - T_g) + \frac{1}{\tilde{M}_C}\sum_{i=1}^{4}\dot{R}''_i\sum_{j=1}^{N}\hat{H}_j(T_s)(b_{ij} - a_{ij})\right) \tag{16}$$

The set of transport equations (8−16), along with boundary and initial conditions, were solved using the Runge−Kutta integration method.

Results and Discussions

The results from the model qualitatively agreed with established patterns (Hobbs et al., 1993) for variations in O_2, CO_2, CO, H_2, and H_2O along the length of the reactor. Predictions were obtained for the conditions listed in Table 1. These were used as the base case in the sensitivity study described below.

For all cases simulated, no more than 20 min was required to reach a pseudo-steady state in which the outlet gas composition and temperature reached constant values. These compositions and the zone thicknesses did not vary until the char bed was nearly

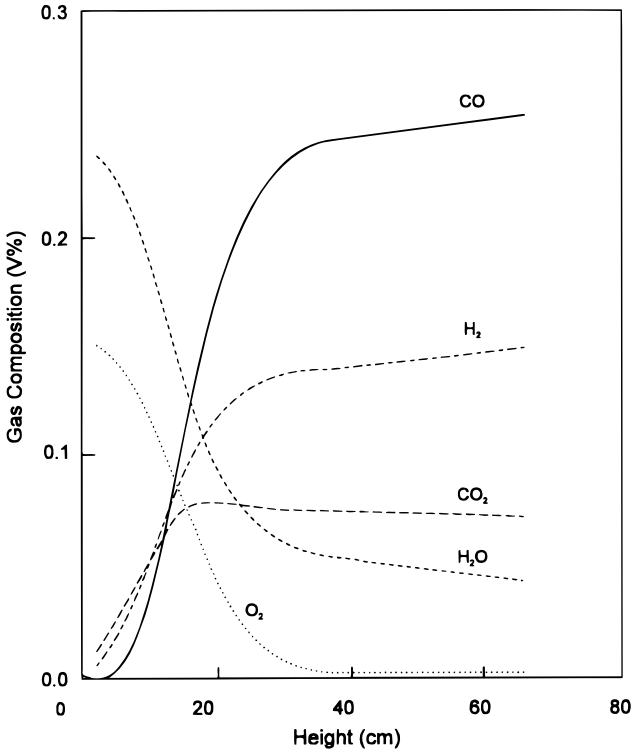

Figure 3. Gas composition profiles along the height of the fixed bed for the base conditions.

Table 1. Base Conditions Used for the Sensitivity Study

P	pressure, kPa	2850
d_p	particle size, cm	0.5
S/A	steam/air ratio	0.2
T_0	initial temp, K	920
$T°_g$	inlet gas temp, K	590
V_g	gas superficial velocity, cm/s	3.0
D	bed diameter, cm	30
L	bed depth, cm	66

entirely consumed. For this reason, all of the dependent variables were evaluated at a time of 20 min after start-up.

The gas composition profile for gasification of char is illustrated in Figure 3. Oxygen was entirely consumed as a result of char combustion, and the CO_2 content of the gas increased with decreasing oxygen content. The maximum level of CO_2 was close to the point of oxygen disappearance; further up in the fuel bed the CO_2 decreased gradually. The formation of CO did not take place appreciably until the CO_2 content was nearly at its maximum. After oxygen disappearance, the CO concentration increased monotonically and reached an almost constant value. Water decomposition started about the same time (location) as CO formation, and the hydrogen content of the gas increased rapidly at first. Following this rapid initial formation, the hydrogen concentration increased more slowly.

The predicted temperature profiles for solids and gases are given in Figure 4. The solids' temperature rapidly increased, reaching a maximum, and then started declining. The gas temperature increased slowly to a maximum, after which it decreased. In the combustion zone, defined as the location where carbon and oxygen coexist (O_2 > 1%), the solids' temperature was much higher than gas temperature. But in the zone above this combustion zone, the gasification zone, the gas temperature was slightly higher than solids' temperature.

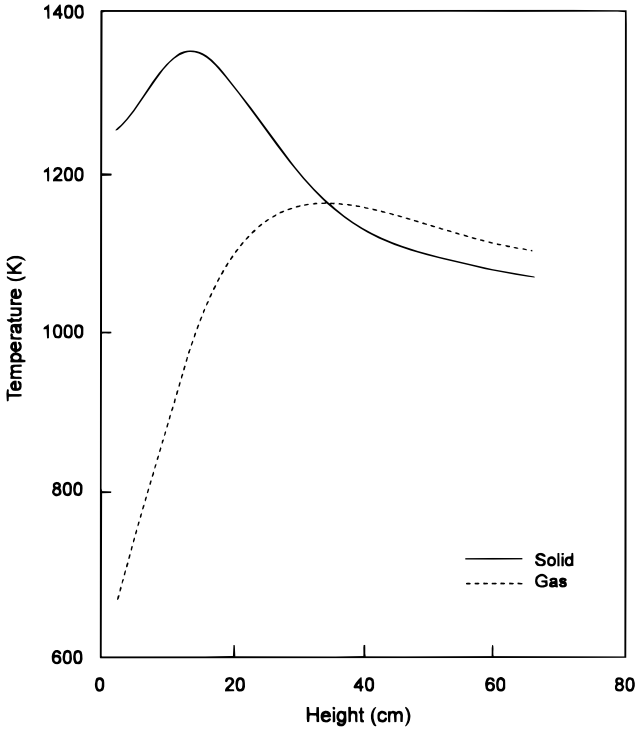

Figure 4. Solid (—) and gas (- - -) temperature profiles as a function of bed height.

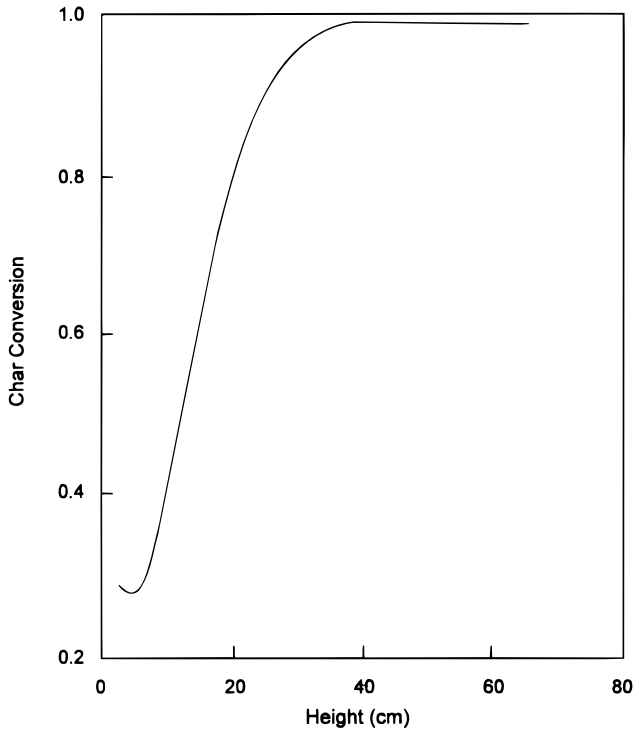

Figure 5. Char conversion profile for the base conditions along the height of the fixed bed.

The variation in char conversion with the position is illustrated by Figure 5. The char conversion was much greater in the combustion zone, where the reaction rate was higher as a result of the high temperature.

The simulations presented here assumed an initial condition with hot solids to simulate the feed in the PyGas process. In addition, this also facilitated char ignition and quicker convergence to a steady state solution. Cases run with lower initial temperatures resulted in a longer time required for ignition of the char

and at temperatures below 700 K the bed did not ignite. At temperatures above 800 K, the high solids' inlet temperature did not affect any of the dependent variables. For conventional gasifiers with coal feed at much lower temperatures, the only dependent variable which will be significantly influenced by the solids' high inlet temperature is the outlet gas temperature. This is merely a result of the heat exchange between the hot gasification products and the inlet coal feed stream.

Sensitivity Study

In order to develop engineering correlations which are generally useful for gasifier operations and design, parametric studies were conducted. The effects of some of the basic operating parameters of the system were studied, such as pressure (P), steam/air ratio (S/A), gas velocity (V_g), inlet gas temperature (T_g), and bed depth (L). Parameters which reflect variations in the feed material were also studied, including particle size (d_p), fuel reactivity (η), and voidage (ϵ). For each of the model input parameters of interest, the others were held constant, while varying the value of the one under study.

Effect of Pressure. Simulations were conducted in which the pressure was varied from atmospheric up to 40 atm due to interest for advanced power applications. The burning rate and combustion zone thickness were strong functions of pressure which increased with increasing pressure. In this study, the thickness of the combustion zone was defined as that length in which the concentration of oxygen dropped below 1%. The relationship between pressure and char burning rate was found to be the following:

$$\frac{\dot{M}_b}{\dot{M}_{b_0}} = \left(\frac{P}{P_0}\right)^{0.85} \tag{17}$$

This dependence of burning rate on pressure agreed very well with the Chukhanov (1963) relationship. Chukhanov's relationship uses the power of 0.83 and is valid for the combustion of a packed bed of carbon particles. By increasing the pressure, the partial pressure of oxygen and steam also increased and caused an increase of carbon conversion.

The combustion zone thickness enlarged with increasing pressure. This strong dependence can be understood by the fact that gas diffusion rates, K_g, for all reactions are inversely proportional to the total pressure. Combustion is a diffusion-rate-limited reaction at these elevated temperatures. Hence, by increasing the pressure, the particle combustion rate decreases; therefore, the width of the combustion zone increased. For the same reason the reaction zone moved up in the bed with increased pressure.

The effect of changing pressure on the solids' maximum temperature and the outlet gas temperature is illustrated in Figure 6. Both variables were strongly dependent on pressure. Increasing the pressure resulted in a substantially increased outlet gas temperature and decreased the solids' maximum temperature. These results were consistent with the experimental results reported by Monson et al. (1995). The decreased solids' maximum temperature is due to the fact that elevated pressure decreases the rate for diffusion-controlled, highly exothermic, oxidation reactions and increases the rate for kinetic-controlled, endothermic,

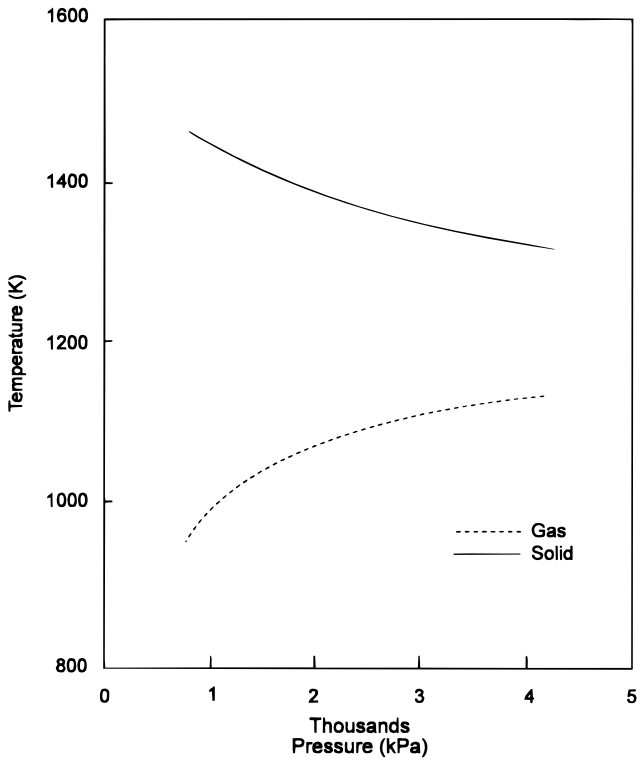

Figure 6. Influence of pressure on maximum solid (—) and outlet gas (- - -) temperatures.

steam gasification reactions (Hobbs et al., 1993). This effect is reinforced by the increased combustion zone thickness, which results in a higher heat transfer area. For this reason, the outlet gas temperature was also increased.

An increase in pressure did not affect the outlet gas higher heating values significantly; increasing the pressure sixfold decreased the gas heating values only 10%.

Effect of Particle Size. The effect of particle size on combustion zone thickness and burning rate is illustrated in Figure 7. The mean particle size was varied between 3 and 8 mm. Typical fixed beds operate with a 6 mm average feed coal, while that for char product from a fluid bed feeding the top of the fixed bed in PyGas was expected to be 3 mm and as small as 1 mm.

As the particle size increased, the width of the combustion zone increased and the char burning rate decreased. These effects were due to the dependence of diffusion-controlled reactions on the available surface area, described by a, the surface area per unit volume (coefficient in eqs 6−14). Gas diffusion rates, K_g, of all reactions are inversely proportional to the particle diameter. Therefore, increasing the particle size decreases the reaction rate, hence increasing the combustion zone size while decreasing the rate of char consumption.

The influence of particle size on the solids' maximum temperature and the outlet gas temperature is illustrated in Figure 8. Decreased solids' maximum temperatures were a direct consequence of reduced oxidation rates due to slower mass transfer. For the same reason the length of the combustion zone widened with larger particles. While the heat transfer coefficient and particle surface area are both inversely related to particle size, the affect of increasing the combustion zone thickness dominates the gas−solid heat transfer

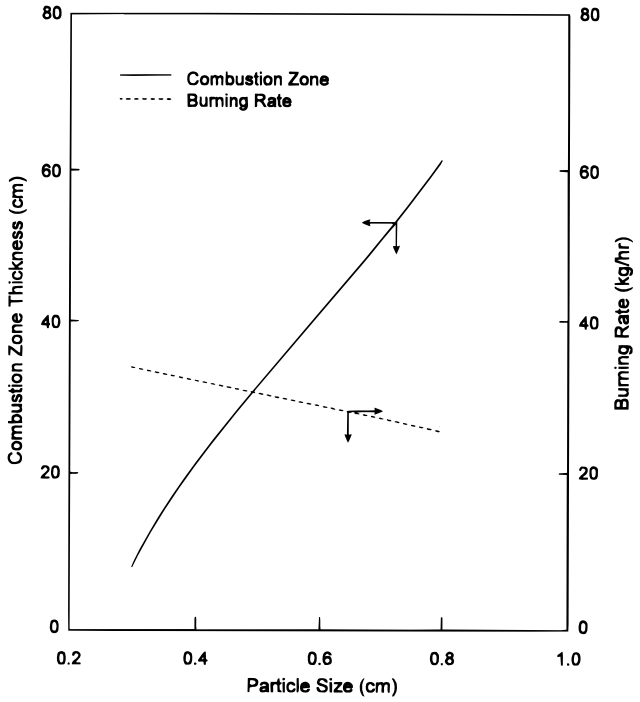

Figure 7. Influence of particle size on the combustion zone thickness (—) and burning rate (- - -).

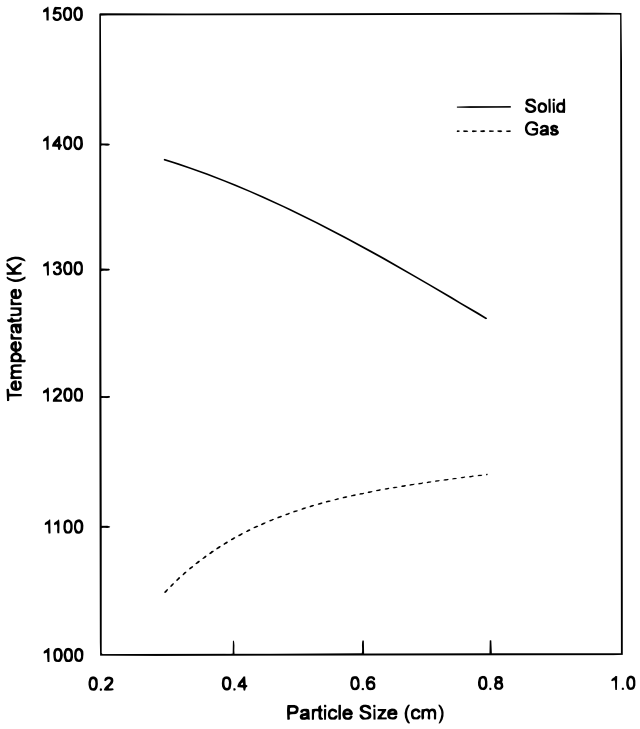

Figure 8. Influence of particle size on the maximum solid (—) and outlet gas (- - -) temperatures.

over the particle size range tested. As a result more heat is transferred from the hot solids to the cooler gas. Thus, the exit gas temperature increased for larger particle size.

The increased particle size did not significantly affect the outlet gas higher heating values; increasing the particle size threefold decreased the gas heating values by only 10%.

Effect of Steam to Air Ratio. One fundamental operating parameter for fixed bed gasifiers is the ratio of steam to air fed under the grate. This operational

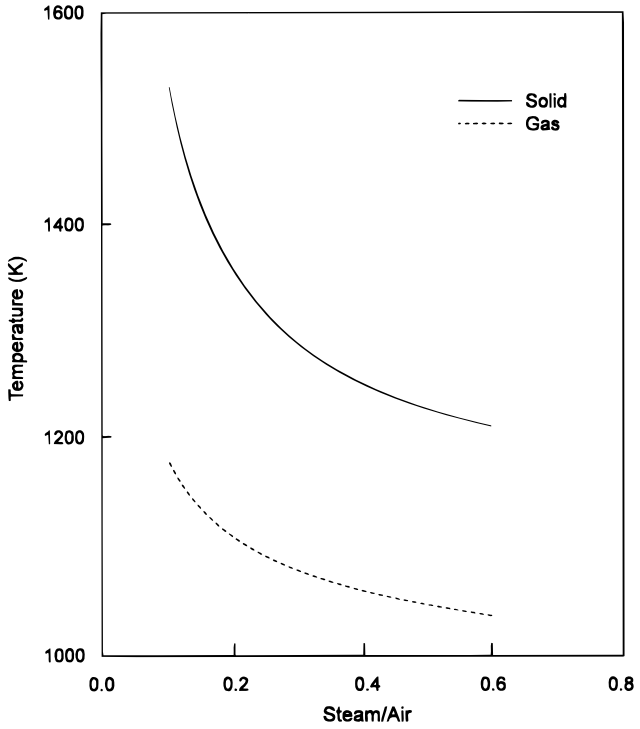

Figure 9. Influence of steam/air ratio on the maximum solid (—) and outlet gas (- - -) temperatures.

parameter is used frequently to control the temperature to avoid significant ash melting (Hobbs et al., 1992). The effect of the steam to air ratio on the solids' maximum temperature and the outlet gas temperature is illustrated in Figure 9. As the steam to air ratio increased, both the solids' maximum and the outlet gas temperatures decreased. Increasing the steam to air ratio also decreased the gas higher heating value due to dilution compared to that quantity required for steam−carbon reaction. This phenomenon is demonstrated by Figure 10.

The combustion zone thickness and burning rate were not greatly affected by an increase in steam to air ratio. This demonstrates the fact that for these conditions the solids' temperature does not have much affect on the combustion rate, i.e., the rate of a gas diffusion-controlled process.

Effect of Bed Depth. The influence of fuel bed depth on water decomposition and outlet gas temperature is illustrated by Figure 11. The height of a fuel bed was varied from 30 to 140 cm. As the depth of the fuel bed was increased, the amount of steam decomposed was increased. As long as the char temperature and reactivity are high enough, the amount of steam which is decomposed can be increased by increasing the depth of the fuel bed. This held true at any given ratio of steam to air. In addition to influencing the amount of decomposed steam, the depth of the fuel bed further affected the composition of the resultant product gas. As the product gas traveled up in the bed, the heating value increased slightly.

The depth of the fuel bed did not affect the combustion zone thickness nor the solids' maximum temperature. However, due to endothermic gasification in the upper bed, increasing the depth of the fuel bed caused a decrease in the outlet gas temperature (Figure 11).

Effect of Air−Steam Blast and Gas Inlet Temperature. The air−steam inlet velocities studied ranged

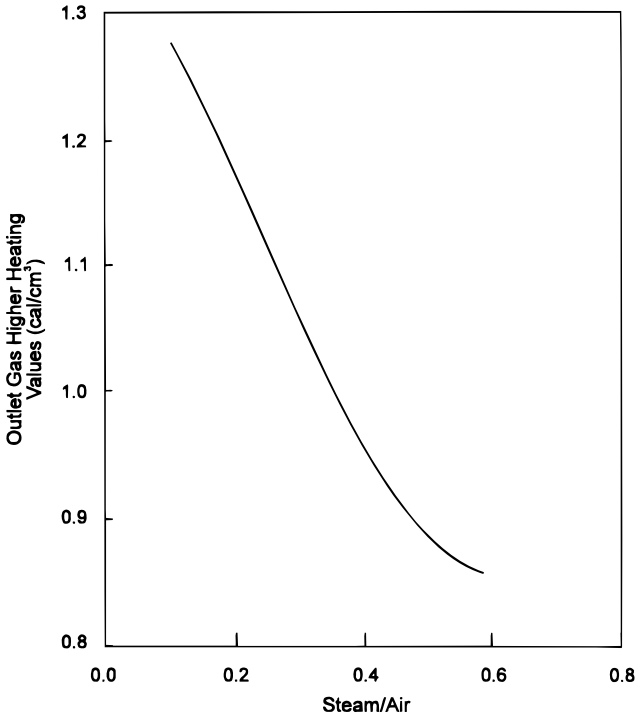

Figure 10. Influence of steam/air ratio on the outlet gas heating values.

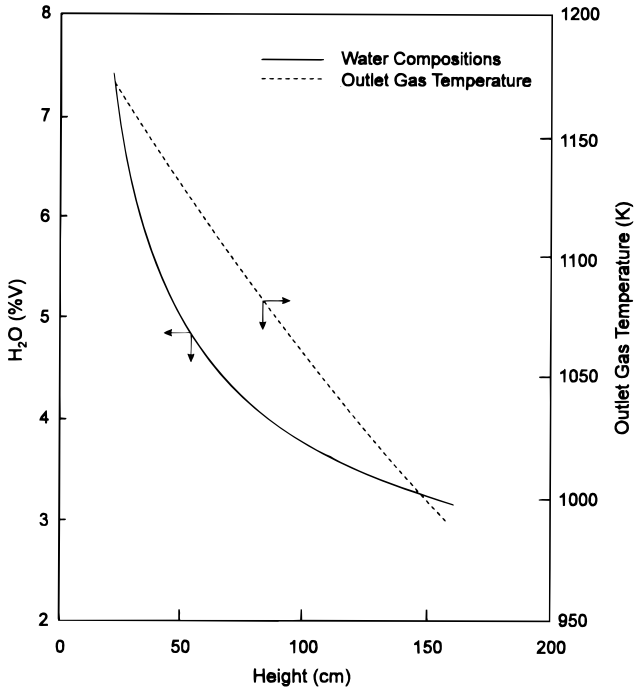

Figure 11. Influence of bed height on water compositions (—) and the outlet gas heating values (- - -).

from 1.5 to 4.6 cm/s. Goldman et al. (1984) reported that, by increasing the air-flow rate in their up-draft gasifier to a high enough value, the reaction zone moved up in the bed ("blow-off"), and it moved back again when the air-flow rate was reduced ("flash-back"). The same effects were qualitatively observed with model simulations, such that as gas velocity increased, the combustion zone moved up in the bed, and the zone moved down with decreased air flows.

Over the range of inlet gas temperatures (530−650 K) studied, the effect of an increase was small but direct,

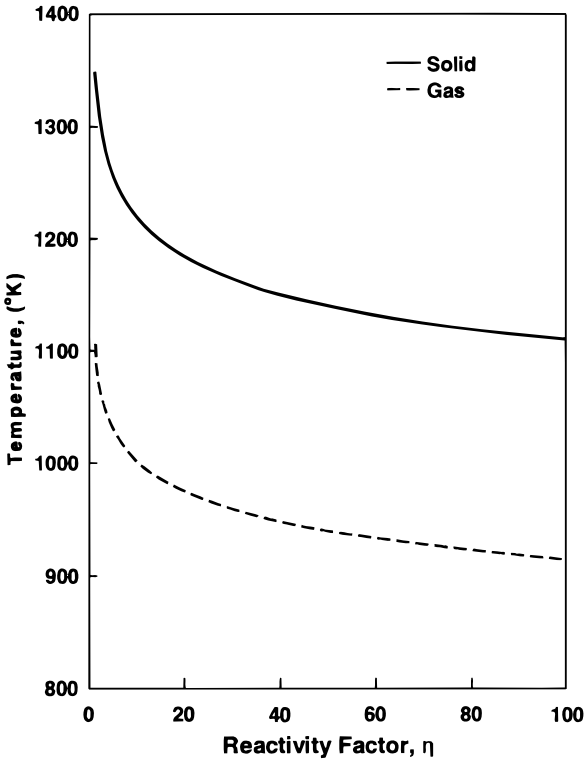

Figure 12. Influence of reactivity on the maximum solid (—) and the outlet gas (- - -) temperatures.

resulting in an increase of the solid's maximum temperature and the rate of gasification, as evidenced by more CO and H_2 in the products. This resulted in a shortened combustion zone length and thereby decreased the relative yields of products of combustion, i.e., CO_2 and H_2O. Over this range of temperatures, a higher inlet gas temperature enhanced the gasification rate, which is kinetically-controlled, more so than the combustion rate, which is diffusion-controlled. As a result, the burning rate actually dropped slightly even though the solid's maximum temperature increased.

Effect of Fuel Feedstock. Reactivity was varied between that of the coke material (low reactivity) and that of the low rank coal (high reactivity) by introducing a reactivity factor, η. This reactivity factor was multiplied by the surface reaction rate constant, K_s, for carbon−steam and carbon−CO_2 reactions (Wen and Chaung, 1979), as reported for bituminous coal chars. The reactivity factor was varied from 0.5 to 100, simulating differences in reactivity from different fuel feedstocks, with $\eta = 1$ for the base condition.

Increased reactivity does not greatly affect combustion rates due to the fact that these reactions are diffusion-controlled. However, the rates of gasification are kinetically-limited, and the reactivity does affect the temperatures and the outlet gas composition. As the reactivity increased, the rate of endothermic reactions also increased, resulting in lower outlet gas and maximum solids' temperatures (Figure 12). The amount of product fuel gases, CO and H_2, increased, while that of diluent gases, CO_2 and H_2O, decreased with increased reactivity. This resulted in a higher gas heating value.

Effect of Bed Voidage. The void fraction in the bed can be modified indirectly when changes are made to the particle size distribution. This, in turn, is determined by the method of sample preparation, crushing, and, in lower rank coals, drying. The range of void

Table 2. Coefficients for the General Linear Model (Eq 19) Correlating Fixed Bed Gasifier Operating Conditions to Performance

			slope							
		independent parameters:	V_g (cm/s)	inlet $T°_g$ (K)	steam−air ratio	D_p (cm)	ϵ	L (cm)	η	P (kPa)
dependent parameter	base value	range: base value:	1.5−4.6 3.0	533−645 589	0.1−0.4 0.2	0.35−0.8 0.48	0.4−0.6 0.5	33−132 66.0	0.5−100 1.0	1400−4300 2860
CO (vol %)	25.7		−0.5	0.0216	−14.2	−2.58	−1.73	2.0	0.63	0.0
CO_2 (vol %)	7.3		0.0	−0.01	7.78	0.0	0.75	−0.23	−0.18	0.0
H_2 (vol %)	14.8		−0.5	0.0054	6.33	−1.19	−1.0	1.44	0.5	−0.0004
H_2O (vol %)	44		0.66	−0.009	9.4	1.49	1.24	−1.8	−0.6	0.0004
burning rate (kg/h)	31.1		8.6	−0.018	0.0	−9.4	−4.0	0.0	0.0	0.0096
comb. length (cm)	30.5		10.0	−0.046	3.96	55.2	31.0	0.0	1.1	0.0096
$T_{s,max.}$ (K)	1352		−2.92	0.365	−200	−112	27.4	0.0	−54.4	−0.03
$T_{g,out}$ (K)	1106		47.3	−0.04	−90.6	55.16	76.2	−105.5	−42.3	0.035

fractions tested was between 0.4 and 0.6. The bed voidage most strongly influenced the length of the combustion zone. For higher bed voidage, oxygen penetrates further through the bed, causing an increased zone thickness. This wider combustion zone resulted in a slightly increased solids' maximum temperature. Also, the wider combustion zone lead to slightly higher relative amounts of CO_2 and H_2O and lower concentrations of CO and H_2.

General Engineering Correlations

Calculations for the design and performance of a coal/char combustor and gasifier are based on energy and mass balances and on equilibrium conditions. Development of models to conduct such calculations and the sensitivity study required for design purposes are complex because of the many variables involved. Therefore, the ability to simplify the time-consuming computational work by the use of mathematical correlations is appealing.

A simplified general linear correlation can be used to relate the dependent variables, π (i.e., burning rate, temperatures, and gas composition), to the design and operating conditions (e.g. inlet gas temperature, steam/air ratio, and pressure).

$$\delta\pi_i = f\left(T°_g, \frac{S}{A}, d_p, v_g, \epsilon, L, P, \eta\right) \tag{18}$$

Applying the chain rule of differentiation to eq 18, it can be shown that

$$\delta\pi_i = \frac{\delta\pi_i}{\mathrm{d}T°_g}\,\mathrm{d}T°_g + \frac{\delta\pi_i}{\delta \ln \frac{S}{A}}\,\delta \ln \frac{S}{A} + \frac{\delta\pi_i}{\delta \ln d_p}\,\delta \ln d_p + \frac{\delta\pi_i}{\delta V_g}\,\delta V_g + \frac{\delta\pi_i}{\delta \ln \epsilon}\,\delta \ln \epsilon + \frac{\delta\pi_i}{\delta \ln L}\,\delta \ln L + \frac{\delta\pi_i}{\delta P}\,\delta P + \frac{\delta\pi_i}{\delta \ln \eta}\,\delta \ln \eta \tag{19}$$

The slope values for each term (i.e., $\delta\pi_i/\delta T°_g$, $\delta\pi_i/\delta(\ln(S/A))$, $\delta\pi_i/\delta(\ln d_p)$, $\delta\pi_i/\delta V_g$, $\delta\pi_i/\delta(\ln \epsilon)$, $\delta\pi_i/\delta(\ln L)$, $\delta\pi_i/\delta P$, and $\delta\pi_i/\delta(\ln \eta)$) were obtained from the results of the sensitivity study and are given in Table 2. In Table 2 the columns are the independent parameters, the terms from the right-hand side of eq 19. The first row of values represents the range over which each independent parameter was varied. The second row is the base value for each. The first column of values represents the values of the dependent variables under the base conditions. The rest of the table presents the slope values, or coefficients, for each independent term in eq 19, which are used to determine the value for the dependent variables, such as gas composition, temperatures, burning rate, and combustion length.

In order to obtain a linear response in the dependent variables (π_i), some of the independent variables (S/A, d_p, ϵ, L, and η) required a transformation, using the natural log function, as shown in eq 19. Multiplying the slope by the deviation from the base conditions for each of the independent variables provides a prediction of the dependent variable. (See Appendix for a sample calculation.)

These correlations were tested for deviations in multiple independent variables, and the results were compared to predictions from the nonlinear transient model. When three and four variables were simultaneously varied within the operating range, the correlations agreed with the model simulations within ±5% error. The combustion length errors were as large as 17%. This was due to the nature of the determination of the zone length. The measurement was prone to a greater uncertainty due to the grid size and shallow oxygen gradient at low concentrations ($[O_2] \approx 1.0$ vol %).

In addition, the linearity of the correlations was evaluated over the range defined in Table 2. The regressions for 60 of the 64 cases (eight dependent variables versus eight independent variables) had a variance explained (R^2 values) greater than 95%. Fifty of the correlations had greater than 98% of the variance explained. The dependence of burning rate on bed voidage and the dependence of outlet gas temperature on particle size had R^2 values of 73%. Two other correlations (inlet gas temperature versus burning rate, and gas velocity versus the solids' maximum temperature) had R^2 values of 91%.

In order to assess the relative importance of each of the variables, a dimensionless index (gain matrix) was generated (Table 3). The values for the gain matrix were obtained by multiplying the slope (i.e., the coefficients from Table 2) by the range differential for the independent variables and dividing by the values of the base conditions for the dependent variables. Table 3 is organized in the same format as Table 2 with the range and base conditions presented in the first two rows and the values at the base conditions in the first column. The remainder of the values in the table represent the normalized gain matrix.

Table 3. Relative Importance (Dimensionless) of Each of the Independent Variables on Dependent Variables in the Gasifier General Linear Model (Eq 19)

			relative importance							
		independent parameters:	V_g (cm/s)	inlet $T°_g$ (K)	steam−air ratio	D_p (cm)	ϵ	L (cm)	η	P (kPa)
dependent parameter	base value	range: base value:	1.5−4.6 3.0	533−645 589	0.1−0.4 0.2	0.35−0.8 0.48	0.4−0.6 0.5	33−132 66.0	0.5−100 1.0	1400−4300 2860
CO (vol %)	25.7		−0.06	0.09	−0.77	−0.083	−0.027	0.11	0.13	0.0
CO_2 (vol %)	7.3		0.0	−0.153	1.48	0.0	0.04	−0.044	−0.13	0.0
H_2 (vol %)	14.8		−0.105	0.041	0.59	−0.067	−0.027	0.135	0.18	−0.078
H_2O (vol %)	4.4		0.46	−0.23	2.96	0.28	0.114	−0.57	−0.07	0.26
burning rate (kg/h)	31.1		0.86	−0.065	0.0	−0.25	−0.05	0.0	0.0	0.89
comb. length (cm)	30.5		1.	−0.17	0.18	1.5	0.2	0.0	0.190	0.91
$T_{s,max}$ (K)	1352		−0.007	0.03	−0.21	−0.069	0.004	0.0	−0.21	−0.064
$T_{g,out}$ (K)	1106		0.133	−0.004	−0.114	0.04	0.014	−0.132	−0.2	0.092

Table 3 provides a quantitative summary of the impact of each of the independent variables on the critical performance parameters. For example, the burning rate was mostly influenced by pressure and the gas velocity, but the particle size effect was only about one-third the magnitude of either pressure or gas velocity. The burning rate is controlled by coal/char combustion, which is a diffusion-controlled process. The other controlled parameters had very little or no influence on burning rate or reactor throughput. Gasification reactivity has little impact on burning rate and throughput in a fixed bed gasifier. As described above, increases in the pressure and velocity and decreases in particle size enhanced the burning rate.

As discussed above, the steam to air ratio had the greatest impact on the product gas composition. As the steam to air ratio increased, the water content of the gas increased at twice the rate of the carbon dioxide content and nearly 5 times that of hydrogen content (Table 3). The other valuable fuel gas product, carbon monoxide, decreased with increasing steam to air ratio. Thus, as well-known in practice, the lower the steam to air ratio, the better the gas quality. The steam−air ratio must therefore be balanced between moderating the maximum temperature, increasing the steam decomposition, and diluting the product value.

The steam to air ratio was the dominant operating parameter which influenced the maximum temperature in the combustion zone (Table 3). This emphasizes the basic premise that steam is principally used in fixed bed gasifiers to moderate the maximum combustion zone temperature. Increasing pressure and particle size had a smaller effect (one-third that of S/A) on the reduction of the maximum char temperature. Voidage and the inlet gas temperature were the only factors which increased maximum temperatures. Their effect was only half that of pressure and particle size.

The need for steam varies with different type coals, such that coals of lower reactivity produced higher maximum combustion temperatures (Table 3). In this case, additional steam would be required to moderate the combustion temperatures. Alternatively, elevated pressure or a decreasing inlet gas temperature could be used to moderate the maximum temperature. The benefit of this would be that a lower steam to air ratio resulted in better product gas quality while higher pressure also increased the burning rate or throughput. Table 3 provides the basis for determining that the pressure changes required would be three times the requirement for changing the steam to air ratio alone.

Likewise, increased particle size in the feed resulted in lower maximum temperature with a gain factor comparable to that of pressure (Table 3). Over the range of conditions considered, the particle size dependence on heat generated (reduction) due to lower combustion rates outstripped the particle size dependence on heat transfer from the solid to the gas.

The next most significant factors influencing the quality of the product gas, after steam to air ratio, were the bed length and the gas velocity (Table 3). As might be expected, the influences of these factors were equal and opposite to each other, such that the higher the length and the lower the gas velocity, the greater the gasification reaction zone and, thus, the greater the utilization of steam and carbon dioxide to produce more hydrogen and carbon monoxide. The effect of these parameters, however, is only one-fifth that of the steam to air ratio. In production of fuel gas products, CO and H_2, the reactivity and particle size had influence comparable to that of either bed length or gas velocity. Increasing the reactivity and decreasing the particle size resulted in increased fuel components in the product gas. On the other hand, increased reactivity decreased CO_2 but had little influence on water production, while increased particle size had little impact on CO_2 but increased the water concentration in the products.

Conclusion

A mathematical model has been presented for gasification of char in a fixed bed. Various operating conditions were considered including P, S/A, V_g, and T_g. With increasing pressure, the combustion zone thickness enlarged and the reaction zone moved up in the bed. Increasing the pressure resulted in a substantially increased outlet gas temperature and a decreased solids' maximum temperature. As the steam to air ratio increased, both the solids' maximum and the outlet gas temperatures decreased. Increasing the steam to air ratio also decreased the gas higher heating value; however, increases in neither the pressure nor the particle size affected the heating values significantly. The combustion zone thickness and burning rate were not greatly affected by an increase in steam to air ratio. However, an increased gas velocity caused the combustion zone to move up in the bed. The effect of an increased inlet gas temperature was small but direct: increasing the solid's maximum temperature and the rate of gasification and yielding more CO and H_2 in the products. This resulted in shortening the combustion zone length.

The effects of the factors leading to bed structure were considered, including L, d_p, and ϵ. As the depth of fuel

bed was increased, the amount of steam decomposed was increased, which increased the heating value and decreased the outlet gas temperature. The depth of the fuel bed did not affect the combustion zone thickness or the solids' maximum temperature. As the particle size increased, the width of the combustion zone increased and the char burning rate decreased. An increased particle size caused a lower solids' maximum temperature, widened the combustion zone, and increased the outlet gas temperature. For higher bed voidage, the combustion zone thickened, the solids' maximum temperature increased, and relatively more CO_2 and H_2O were produced.

Also, the affect of varying the feedstock was considered. Increased reactivity did not greatly affect combustion rates; however, the outlet temperature drops off and the gas quality improves. The reasons for these trends are discussed.

A mathematical correlation resulting from the sensitivity analysis is presented for calculating the effect of any single variable or combination of variables in the gasification of char with air and steam and for pressure as high as 4200 kPa. It is shown that gasifier performance can be predicted rapidly for a given set of conditions. The general correlation was used to obtain the relative effects of different variables which influence a fixed bed gasifier. The correlation also provided ready means for the rapid prediction of the performance of a gasifier in which char is gasified by means of air and steam.

Acknowledgment

The authors would like to acknowledge the Department of Energy for funding the research through the Fossil Energy's Integrated Gasification Combined-Cycle program. In addition, the authors would like to acknowledge Richard Sadowski from Jacobs-Sirrine Engineers, Inc. for his encouragement throughout this research.

Appendix (Illustrative Examples Using General Linear Model)

Example. Find the percentage volume of CO, CO_2, H_2, and H_2O, and also calculate the maximum combustion temperature, the combustion zone thickness, the outlet gas temperature, and the burning rate produced by burning char for the following conditions: $V_g = 3.0$ cm/s, $P = 2169$ kPa, $S/A = 0.3$, $\eta = 10$, $d_p = 0.48$ cm, $L = 66$ cm, and $T°_g = 589$ K.

Solutions. The comparison between the base and the given condition shows that the gasifier pressure, S/A, and reactivity are varied from the base conditions; therefore, by using eq 19 and Table 2 the following results are obtained:

$$\%CO = 25.7 + 0.0(2169 - 2860) + (-14.2)(\ln(0.3) - \ln(0.2)) + 0.63(\ln(10) - \ln(1)) = 21.4\%$$

$$\%CO_2 = 7.3 + 0.0(2169 - 2860) + 7.78(\ln(0.3) - \ln(0.2)) + (-0.18)(\ln(10) - \ln(1)) = 10.1\%$$

$$\%H_2 = 14.8 + (-0.0004)(2169 - 2860) + 6.33(\ln(0.3) - \ln(0.2)) + 0.5(\ln(10) - \ln(1)) = 18.8\%$$

$$\%H_2O = 4.4 + 0.0004(2169 - 2860) + 9.4(\ln(0.3) - \ln(0.2)) + (-0.6)(\ln(10) - \ln(1)) = 6.6\%$$

$$T_{max} = 1352 + (-0.03)(2169 - 2860) + (-200)(\ln(0.3) - \ln(0.2)) + (-54.4)(\ln(10) - \ln(1)) = 1166 \text{ K}$$

$$T_g = 1106 + 0.035(2169 - 2860) + (-90.6)(\ln(0.3) - \ln(0.2)) + (-42.3)(\ln(10) - \ln(1)) = 948 \text{ K}$$

$$L_c = 30.5 + 0.0096(2169 - 2860) + 3.96(\ln(0.3) - \ln(0.2)) + 1.1(\ln(10) - \ln(1)) = 28.0 \text{ cm}$$

$$M_b = 31.1 + 0.0096(2169 - 2860) + 0.0(\ln(0.3) - \ln(0.2)) + 0.0(\ln(10) - \ln(1)) = 24.5 \text{ kg/h}$$

The transient model predicted the following: CO = 20.2%, CO_2 = 11.1%, H_2 = 19.6%, H_2O = 6.4%, T_{max} = 1165 K, T_g = 960 K, L_c = 26 cm, and M_b = 24.4 kg/h.

As shown above the results obtained from the general linear model agree well with the prediction of the transient model.

Nomenclature

a = contact area per unit volumes (cm^2/cm^3)
a_{ij} = molar stoichiometric coefficient of reactant gas species j in reaction i
b_{ij} = molar stoichiometric coefficient of product gas species j in reaction i
C_{pg} = specific heat of gas (cal/g·K)
C_{ps} = specific heat of solid (cal/g·K)
d_p = particle size (cm)
h = heat transfer coefficient ($cal/cm^2 \cdot s \cdot K$)
$\hat{H}_j$ = molar enthalpy of gas species j (cal/g·mol)
K_{ash} = ash diffusion rate constant ($g/cm^2 \cdot s \cdot kPa$)
K_g = gas film reaction rate constant ($g/cm^2 \cdot s \cdot kPa$)
K_s = surface reaction rate constant ($g/cm^2 \cdot s \cdot kPa$)
L = bed depth (cm)
L_c = combustion zone thickness (cm)
$\dot{m}''$ = mass flux of gas species ($g/cm^2 \cdot s$)
$\tilde{M}$ = molecular weight of gas species (g/g·mol)
$\dot{M}_b$ = burning rate of carbon (g/s, cm/s, or cm^3/s)
$\tilde{M}_c$ = molecular weight of carbon (g/g·mol)
N = total number of gas species involved in gasification
P = pressure (kPa)
$P_j - P^*_j$ = effective partial pressure of the jth component (kPa)
$\dot{R}''_i$ = reaction rate of eq i ($i = 1-4$) ($g/cm^2 \cdot s$)
S/A = steam/air ratio (kg/kg)
t = time (s)
T_g = gas phase temperature (K)
$T°_g$ = inlet gas temperature (K)
T_s = solid phase temperature (K)
V_g = gas velocity (cm/s)
y = system axis (cm)

Greek Letters

ϵ = void fraction
ϵ_a = void fraction in ash layer
ξ = fraction of the particle radius which is occupied by unreacted char (cm/cm)
η = reactivity factor (fraction of base value)
ρ_g = gas density (g/cm^3)

ρ_s = solid density (g/cm^3)
ϕ = mechanism factor

Literature Cited

Arthur, J. R. Reaction Between Carbon and Oxygen. *Trans. Faraday Soc.* **1951**, *47*, 164.

Brown, M. J.; Sadowski, R. S. The PyGas Process, as Modeled by DOE-MGAS & KRW Kinetic Rate Equations. International Power Generation Conference, San Diego, CA, October 1991.

Cho, Y. S. Modeling and simulation of Lurgi-type gasifier. M.S. Thesis, Washington University, St. Louis, 1980.

Chukhanov, Z. F. Heat and Mass Transfer Between Gas and Granular Material. *Int. J. Heat Mass Transfer* **1963**, *6*, 691.

Cooperman, J.; Davis, J. D.; Seymour, W.; Ruckes, W. L. *Lurgi Process: Use for Complete Gasification of Coals with Steam and Oxygen Under Pressure*; Bulletin 498; Bureau of Mines: 1951.

Field, M. A.; Gill, D. W.; Morgan, R. B.; Hawskley, P. B. W. Combustion of Pulverized Coal. *Br. Coal Utilization Res.* **1967**, *31* (6), 285.

Goldman, J.; Xieu, D.; Oko, A.; Milne, R.; Essenhigh, R. H. A Comparison of Prediction and Experiment in the Gasification of Anthracite in Air and Oxygen-Enriched/Steam Mixtures. *20th Int. Symp. Combust.* **1984**, 1365.

Gupta, A. S.; Thodos, G. Direct Analogy Between Mass and Heat Transfer to Beds of Spheres. *AIChE J.* **1963**, *9*, 751.

Hobbs, M. L.; Radulovic, P. T.; Smoot, L. D. Modeling Fixed-Bed Coal Gasifier. *AIChE J.* **1992**, *38*, 681.

Hobbs, M. L.; Radulovic, P. T.; Smoot, L. D. Combustion and Gasification of Coals in Fixed-Beds. *Prog. Energy Combust. Sci.* **1993**, *19*, 505.

Hubmann, O. Advances in the technique of gasifying fine, high-ash coal under pressure. International Conference on Complete Gasification of Mined Coal, Liege, May 1954.

Monazam, E. R. A theoretical and experimental investigation of coke gasification in a batch reactor. Ph.D. Dissertation, West Virginia University, Morgantown, WV, 1986.

Monazam, E. R.; Johnson, E. K.; Zondlo, J. W. Modeling and Simulation of a Cross-flow Coal Gasifier. *Fuel Sci. Technol. Int.* **1992**, *10* (1), 51.

Monson, C. R.; Germane, G. J.; Blackham, A. U.; Smoot, L. D. Char Oxidation at Elevated Pressure. *Combust. Flame* **1995**, *100*, 669.

Reed, T. B.; Markson, M. A Predictive Model for Stratified Downdraft Gasification of Biomass. In *Progress in Biomass Conversion*; Tillman, D. A., Jahn, E. C., Eds.; Academic Press: New York, 1983; Vol. 4.

Von Fredersdorff, C. G.; Elliott, M. A. In *Chemistry of Coal Utilization*; Lowry, H. H., Ed.; John Wiley: New York, 1963; Supplementary Volume, p 892.

Wen, C. Y. Noncatalytic Heterogenous Solid Fluid Reaction Models. *Ind. Eng. Chem.* **1968**, *60* (9), 34.

Wen, C. Y. *Optimization of Coal gasification Processes*; R & D Report No. 66; Office of Coal Research: Washington, DC, 1972.

Wen, C. Y.; Chaung, T. Z. Entrainment Coal Gasification Modeling. *Ind. Eng. Chem. Process Des. Dev.* **1979**, *18*, 684.

Wen, C. Y.; Dutta, S. In *Coal Conversion Technology*; Wen and Lee, Eds.; Addison-Wesley Pub. Co.: 1979; Vol. 2, p 141.

Yoon, H.; Wei, J.; Den, M. M. A Model for Moving-Bed Coal Gasification Reactors. *AIChE J.* **1978**, *25*, 429.

Received for review March 18, 1997
Revised manuscript received September 30, 1997
Accepted September 30, 1997[⊗]

IE970229W

[⊗] Abstract published in *Advance ACS Abstracts*, December 1, 1997.